16TH EUROPEAN CONFERENCE ON EARTHQUAKE ENGINEERING THESSALONIKI 18 - 21 JUNE 2018

THE IMPACT OF VIBRATION-CONTROLLED SYSTEMS IN CATASTROPHE MODELLING

Alin RADU[1], Irina F. LAZAR[2]

ABSTRACT

Catastrophe (CAT) modelling is a field that combines science and engineering to assess natural and man-made catastrophe risk to allow the risk-takers to better understand and manage their risks. CAT modelling has an essential role in the (re)insurance industry, in which probabilistic models are used to quantify the risk of perils, such as earthquakes. The purpose of this paper is to analyse whether the implementation of vibration-control systems can reduce the seismic risk.

The CAT modelling framework described in this paper is for a hypothetical settlement, located in a seismic zone. Three main components are essential in CAT modelling: the hazard, the exposure, and the engineering parts, each modelled, in this paper, using simplified approaches. The seismic hazard is described by a probabilistic model for earthquakes characterized by two parameters, the moment magnitude and the epicentral distance. The exposure is represented by a deterministic distribution of buildings idealized as single-degree-of-freedom linear and non-linear systems. Finally, the engineering part develops two sets of empirical vulnerability curves for the vibration-uncontrolled and controlled systems, using a dataset of real ground-motion records. The seismic risk of the portfolio of controlled and uncontrolled systems will be evaluated in terms of metrics used in CAT modelling, such as the annual average loss, and the exceedance-probability curves, which indicate the loss expected to occur at given intervals of time.

Keywords: Catastrophe Modelling; Seismic risk assessment; Tuned-inerter damper;

1. INTRODUCTION

Catastrophe models are complex computer-aided representations of the risk assumed by a portfolio of assets due to natural or man-made catastrophes (AIR Worldwide, 2017). This paper focuses on the quantification of the earthquake risk. The catastrophe modelling framework for earthquakes is similar to the probabilistic seismic hazard analysis, and it estimates the risk of buildings located in a seismic area by accounting for the uncertainty in the seismic hazard, location of buildings and structural behaviour. The catastrophe modelling framework is used in the insurance industry to estimate the risk of assets in terms of monetary losses, by building models for the seismic hazard, the exposed assets, and the vulnerability of structures. Catastrophe models and their outputs may also be used in the management and the decision-making for the disaster risk (Goda K, 2015; Poliquin B, Lalonde D, 2012).
The goal of this paper is to use the catastrophe-modelling framework for earthquakes to evaluate the seismic risk of a portfolio of assets and the influence that the installation of vibration-control systems could have on the seismic risk. In this paper, the tuned-inerter damper (TID) is chosen as the vibration-suppression system to be modelled inside selected non-linear Duffing SDOF structures. This is a passive control system proposed in Lazar et al. (2014). The TID has a layout similar to that of passive tuned-mass-dampers (TMD), where the mass element is replaced with an inerter. This device was introduced by Smith and its functioning is explained in detail in Smith (2002). Extensive research

[1]Marie Skłodowska-Curie Research Fellow, Department of Civil Engineering, University of Bristol, Bristol, UK, alin.radu@bristol.ac.uk
[2]Senior Research and Teaching Associate, Department of Mechanical Engineering, University of Bristol, Bristol, UK, irina.lazar@bristol.ac.uk

into the use of inerter-based vibration-control systems in civil engineering applications have been carried out recently, for example Marian and Giaralis (2014), Lazar et al. (2016), Giaralis and Taflanidis (2017) or Gonzalez-Bulega et al. (2017).
A simplified hypothetical scenario is used for this study, by looking at all four main components of the catastrophe-modelling framework, i.e. the hazard, the exposure, the vulnerability and the financial part. Each component is described separately and integrated in the framework for the evaluation of the two views of the risk. The seismic hazard is assumed to be generated by hypothetical seismic sources used to generate seismic events using Monte Carlo simulations. A simple ground-motion prediction model (Abrahamson NA, Silva WJ, 1997) is used for the evaluation of the local intensity of each seismic event. The exposure part is deterministic and describes the spatial distribution and the type of exposed assets. The types of buildings in the exposure are modelled as linear and non-linear Duffing single-degree-of-freedom (SDOF) oscillators. For the vulnerability component, the NGA-West dataset of ground motions is used to construct empirical vulnerability curves for the types of assets considered. Finally, the financial losses are evaluated in terms of annual average losses and average losses at specified return periods.
The efficiency of the TID system adopted for the reduction of the seismic risk in the selected assets is discussed in terms of the two types of financial outputs. Numerical examples are presented in the paper for the considered scenario by varying the number of TID-controlled assets.

2. SEISMIC RISK IN VIBRATION CONTROLLED-SYSTEMS

The most common tool used in the seismic-risk evaluation is the seismic fragility, which represents the probability that a dynamic system enters a critical damage state for given levels of the seismic intensity measure. Fragility curves are graphical representations of seismic fragilities, most commonly as functions of spectral values of the response acceleration. This section calculates empirical fragility curves for three types of systems used in the catastrophe-modelling framework described below. The following equations describe the response $X(t)$ of the linear and the Duffing single-degree-of-freedom (SDOF) oscillators to the input $A(t)$:

$$\ddot{X}(t) + 2\xi\upsilon\dot{X}(t) + \upsilon^2 X(t) = -A(t), \tag{1}$$

$$\ddot{X}(t) + 2\xi\upsilon\dot{X}(t) + \upsilon^2 (X(t) + \varepsilon X(t)^3) = -A(t), \tag{2}$$

where υ, ξ in Equations 1 and 2 are the natural frequency and the damping ratio for the linear SDOF system, and ε in Equation 2 is a system parameter that accounts for the cubic non-linearity of the Duffing oscillator. Note that for $\varepsilon = 0$, Equations 1 and 2 are identical. For the numerical examples in this paper, the following values are employed as parameters: $\upsilon = 2\pi/0.3$ rad/s, $\xi = 0.05$ and $\varepsilon = -500$.

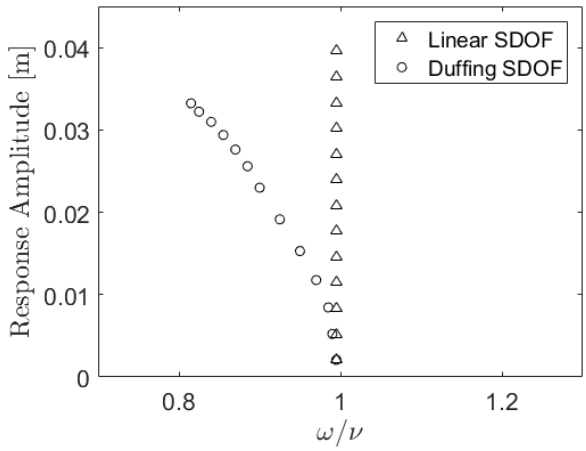

Figure 1. Backbone curves for the linear and Duffing SDOF oscillators.

The behaviour of the systems in Equations 1 and 2 is described by the backbone curves shown in Figure 1, which are plots of the maximum response amplitudes $\max_{t\geq 0}|X(t)|$ to harmonic excitations of the form $a\sin(\omega t)$, for a range of forcing frequencies, ω, and acceleration amplitudes, a. Since the non-linear system reaches its maximum amplitudes at lower frequencies, and thus has a lower performance under seismic excitation, a vibration suppression system to be modelled inside non-linear host structures is presented in the next subsection.

2.1 Tuned-Inerter Damper

The assets forming the portfolio analysed in this paper are modelled as linear and nonlinear SDOF structures. Part of the nonlinear structures are equipped with TIDs. These structures are more vulnerable to seismic excitation given the presence of the softening effect shown in Figure 1 (triangular markers). As detailed in Lazar et al. (2014), the TID introduces an extra DOF and the response of the TID-controlled system is described by Equations 3 and 4.

$$\ddot{X}(t) + 2\xi\upsilon\dot{X}(t) + \upsilon^2(X(t) + \varepsilon X(t)^3) + 2\xi_{TID}\upsilon_{TID}\mu\left(\dot{X}(t) - \dot{Y}(t)\right) + \upsilon_{TID}^2\mu\big(X(t) - Y(t)\big) = -A(t) \quad (3)$$

$$\ddot{Y}(t) + 2\xi_{TID}\upsilon_{TID}\left(\dot{Y}(t) - \dot{X}(t)\right) + \upsilon_{TID}^2\big(Y(t) - X(t)\big) = 0. \quad (4)$$

where ξ_{TID} and υ_{TID} are the TID damping ratio and natural frequency respectively, and μ is the inertance-to-mass ratio between the TID and the host structure. These parameters are tuned to ensure minimum acceleration response of the TID-controlled structure subjected to base acceleration, as detailed in Gonzalez-Buelga et al. (2017).

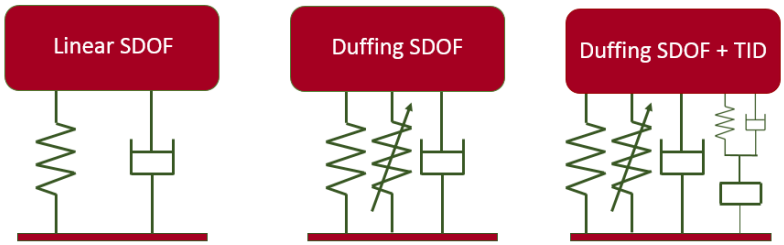

Figure 2. Structural systems.

2.2 Empirical Fragility Curves

Fragility curves for the systems in Equations 1, 2 and 3 are calculated as graphical representations of the probability

$$P_f(im) = \boldsymbol{P}\left\{\max_{t\geq 0}|X(t)| > x_{cr}\,|IM = im\right\}, \quad (4)$$

where $X(t)$ is the response of the systems in Equations 1, 2 or 3 to the input ground motion $A(t)$ characterized by the intensity measure $IM = im$, such as the peak ground acceleration or the spectral ordinates of the structural response. In this case, the intensity measure is the pseudo-spectral acceleration $IM{=}\upsilon^2\max_{t\geq 0}|X(t)|$, where $X(t)$ is the response of the linear SDOF systems in Equations 1, characterized by $\upsilon = 2\pi/0.3$ rad/s and $\xi = 0.05$. The empirical fragility curves are calculated using the dynamic responses of these systems subjected to the ground motions in the NGA-West database of earthquakes. Every earthquake $a_k(t), k = 1, \ldots, N$ in the dataset can be seen as a sample of the input process $A(t)$. Thus, Equation 4 can be rewritten as

$$P_f(im_i) = \frac{1}{N_i}\sum_{k=1}^{N} \mathbf{1}\left\{\max_{t\geq 0}|x_k(t)| > x_{cr}\right\}\mathbf{1}\{im_k \in \Omega_i\}, \quad (4)$$

where im_k is the pseudo-spectral acceleration of ground motion $a_k(t)$, and Ω_i is an interval centred around the value im_i. Due to the limited amount of data available, $P_f(im_i)$ cannot be calculated at many values of im_i, and, thus, the fragility function described in Equation 4 is a discrete, scattered function. Therefore, lognormal cumulative distribution functions fitted to the data calculated from Equation 4 are used for fragility functions (Vamvatsikos D, Cornell A, 2002). Fragility functions calculated for $x_{cr} = 0.035$ are shown in Figure 3 for all the systems considered.

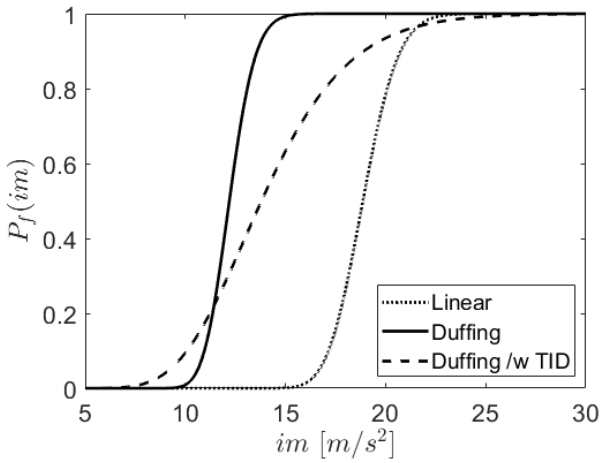

Figure 3. Fragility functions calculated for $x_{cr} = 0.035$

The performance of the Duffing systems is reduced when the TID is installed intensities in the range of 4 to 11 m/s^2, but the TID-controlled Duffing systems performs considerably better at higher intensities. Note that this observation is valid for the chosen threshold and the performance of the systems depends significantly on the damage state considered, i.e. the magnitude of x_{cr}, in this current case.

3. CATASTROPHE MODELLING FRAMEWORK

The catastrophe modelling framework, schematically represented in Figure 4 (AIR Worldwide, 2017), is composed of four main parts: the hazard, the exposure, the vulnerability and the financial components. Each part of the framework is described independently in this section.

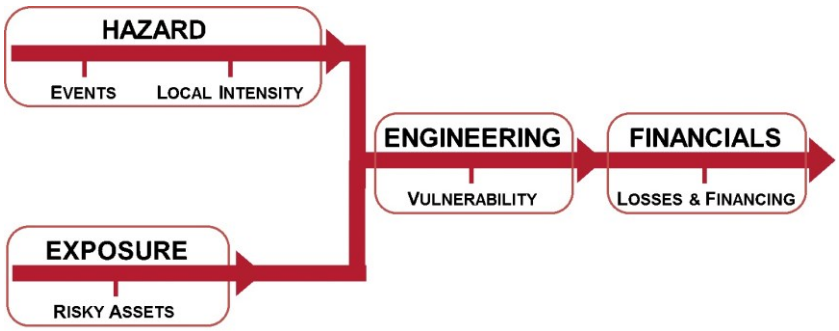

Figure 4. Catastrophe modelling framework

The framework shown in Figure 4 is used to produce outcome that can be used to evaluate the performance of vibration-control devices installed for a large portfolio of assets.

3.1 Hazard

The hazard part of the earthquake catastrophe-modelling framework consists of two parts: the seismic-event simulation, and the local-intensity calculation. Simple models are used to characterize the seismic hazard for a hypothetical site, described in the left panel of Figure 5. The black dots in the rectangular area represent the assets exposed to the seismic risk generated by two types of seismic sources: (1) fault lines, represented by solid black lines, and (2) background seismicity, represented by a distribution (concentric coloured ellipses) of the location of the epicentres outside the fault lines. For this study, the earthquake events are characterized only by the location of the epicentre and their moment magnitude.

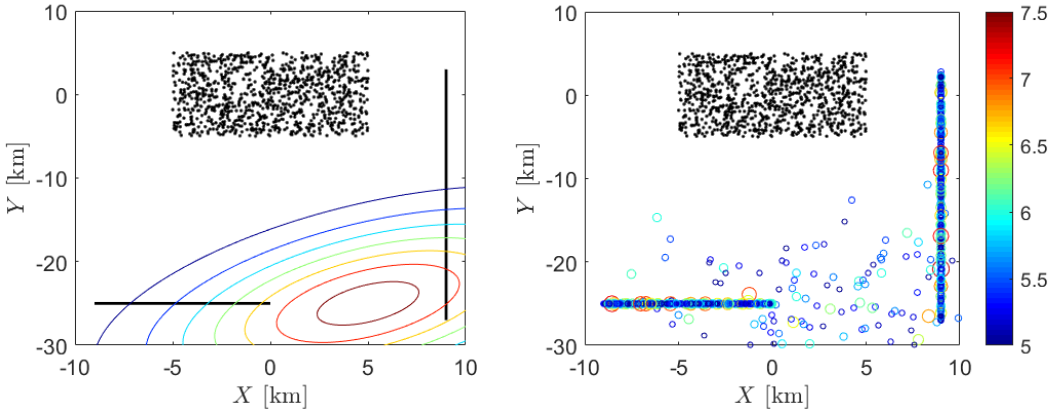

Figure 5. Seismic-hazard sources (left); 1,000-event earthquake catalog of events distributed by location and moment magnitude (right)

The point locations of earthquakes along the fault lines are assumed to be uniformly distributed, while the sources assumed by the background seismicity follow the distribution shown in Figure 5. The moment magnitudes of the earthquakes, irrespective of the source, follow the Guttenberg-Richter distribution:

$$f_M(m) = \frac{b10^{-b(m-m_{min})}\ln(10)}{1-10^{-b(m_{max}-m_{min})}}, \tag{4}$$

where $b = 1$ and the minimum and maximum magnitudes considered are $m_{min} = 5$, and $m_{max} = 8$, respectively. Figure 5 (right) shows 1,000 events with magnitudes represented by the colour scheme on the right side and also by the size of the circles marking each event, also known as a *1000-event earthquake catalogue*, in the insurance industry.

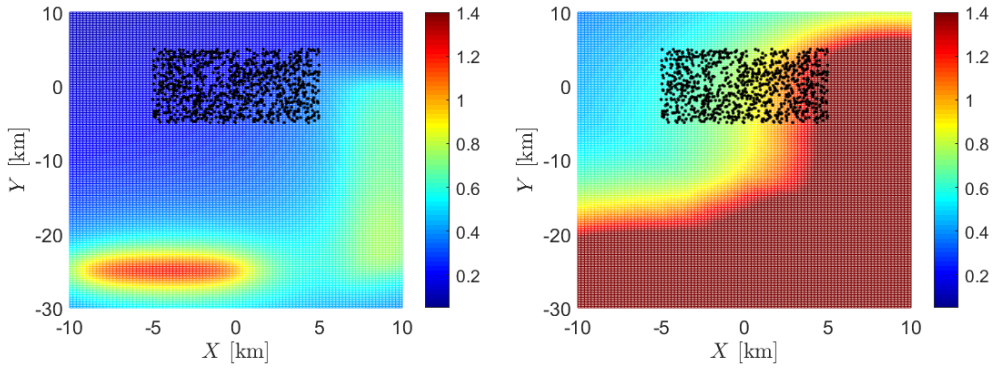

Figure 6. 10-year (left) and 1,000-year (right) return-period $SA(0.3s; 0.5\%)$ hazard maps

The local intensity for each event is calculated using a simple, relatively old, ground-motion prediction equation developed by Abrahamson and Silva (1997), which suffices for the purpose of this study. Figure 6 shows the 10-year and the 1,000-year return-period hazard maps, respectively, for the pseudo-spectral acceleration calculated for a period of 0.3 s and a damping ratio of 5%.

3.2 Exposure

The exposure represents a collection of 1,000 assets exposed to the seismic risk. A simple model is used in this case, as already presented in Figure 5. The locations of the assets are given by a sample of the bi-variate uniform distribution between [-5, 5] km coordinated along the X and Y Cartesian coordinates. The assets are assumed to be of two types, as shown in the left panel of Figure 7. The blue dots are the assets whose dynamic behaviour is characterized by the linear SDOF system in Equation 1, while the red dots are the assets whose dynamic behaviour is characterized by the Duffing SDOF system in Equation 2.

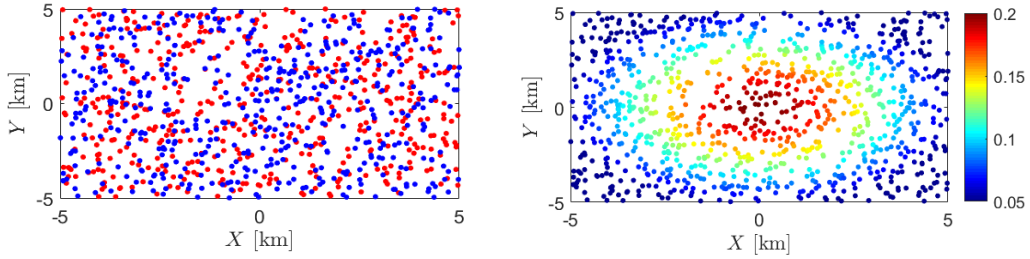

Figure 7. Spatial distribution of the exposure type (left), and value (right)

The distribution of the monetary value of each asset is given by a bi-variate normal distribution probability density function, as shown in the left panel of Figure 7. The values have been normalized such that the total value of the assets to sum up to 100.

3.3 Engineering

The engineering part of the catastrophe-modelling framework describes how vulnerable buildings are for given levels of ground-motion intensities. A practical tool for this description are vulnerability curves, which are similar to the fragility curves described in Section 2.2. Like fragility curves, vulnerability curves are functions of the ground-motion intensity measures. Unlike fragility curves, which are representations of the probability of exceedance of a critical limit (in this case a maximum absolute displacement), vulnerability curves are representations of the mean damage ratios. Mean damage ratios are the ratios between the value of the repair over the total value of the asset. Usually, mapping between fragility and vulnerability curves is estimated using insurance-claim data, but for simplicity we assume that the vulnerability curves are identical with the fragility curves shown in Figure 3. Thus, for the purpose of this paper, the value $P_f(im)$ represents the ratio between the cost of repair of an asset damaged at the intensity measure im and the total cost of the asset.

The linear and Duffing SDOF systems perform significantly different for the chosen parameters, as seen in Figure 3. Since the performance of the Duffing SDOF is poorer than the one of the linear SDOF, a strategy of installing TID in the Duffing SDOF systems is adopted. Thus, in order to study the efficiency of TIDs, the catastrophe-risk framework will be run twice for the exposure with and without a TID modelled inside the Duffing systems. Note that installing the TID in the Duffing systems comes at the expense that this system will underperform at lower values of the intensity measure, as noted already in Section 2.2.

3.4 Financials

Two financial metrics are usually employed in the insurance industry, that is, average losses and losses

associated with given exceedance probability. In order to calculate losses, the hazard, exposure and engineering parts are combined using the following algorithm:

Step1: Simulate N_{ev} samples of earthquake events, i.e. $(m_k, x_k, y_k), k = 1, \dots, N_{ev}$, where m_k are moment magnitude samples from the distribution in Equation 4 and (x_k, y_k) are coordinates of the epicentre for event k, simulated from the uniform distributions along the line faults or the distribution assumed for the background seismicity;

Step2: For every event k in the catalogue, calculate the distances $r_{k,i}$ from the epicentre to the location of every asset $i = 1, \dots, N_{ex}$ in the exposure, where N_{ex} is the total number of assets in the exposure;

Step3: Calculate the intensity measure, i.e. the pseudo-spectral acceleration, $im_{k,i}$ for the frequency $\upsilon = 2\pi/0.3$ rad/s and damping ratio $\xi = 0.05$, using a ground-motion prediction equation with the input $(m_k, r_{k,i})$ for every exposure location;

Step4: Calculate the loss for every event $k = 1, \dots, N_{ev}$ and every asset $i = 1, \dots, N_{ex}$ as

$$l_{k,i} = v_i P_f(im_{k,i}), \tag{5}$$

where $v_i, i = 1, \dots, N_{ex}$ is the value of asset i, as described in Figure 7 (left).

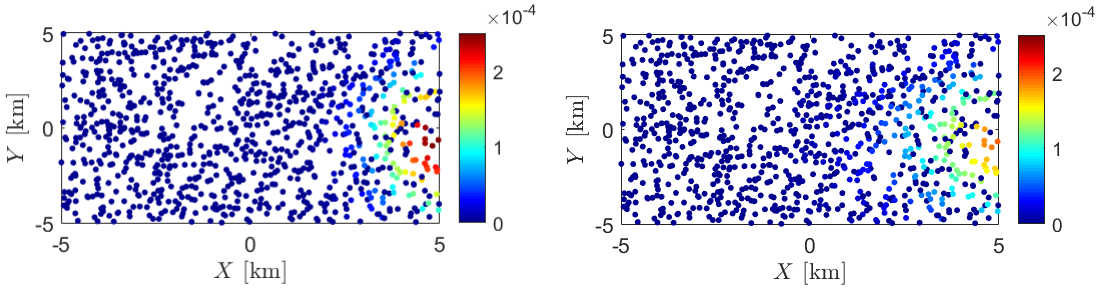

Figure 8. Average losses for the original exposure (left) and the TID-controlled exposure (right)

Finally, the average loss at each location is calculated as

$$L_i = \frac{1}{N_{ev}} \sum_{k=1}^{N_{ev}} l_{k,i}, \tag{6}$$

and the probability that the total losses exceed a given value l is

$$\boldsymbol{P}\{L > l\} = \frac{1}{N_{ev}} \sum_{k=1}^{N_{ev}} \mathbf{1}\left\{\sum_{i=1}^{N_{ex}} l_{k,i} > l\right\}. \tag{7}$$

For the numerical examples in this study, $N_{ev} = 100{,}000$ simulations of seismic events were used to calculate losses for $N_{ex} = 1{,}000$ assets, whose value summed up to $V = \sum_{i=}^{N_{ex}} v_i = 100$. Figure 8 shows the average losses L_i spatially distributed at asset locations, for the original structures (left) and the exposure with the TID-controlled Duffing systems (right). It is noticed that the average losses of the assets located between $x \in [4,5]$ km are reduced. However, the spread of the average losses for the Duffing systems increases when these systems are controlled, i.e. average losses of the TID-controlled Duffing systems in the area located between $x \in [2,3]$ km increase in comparison to the uncontrolled Duffing systems. These results are expected since most of the contribution in the average losses is given by many small events, for which the TID-controlled systems underperform, as seen in the fragility curves in Figure 3, for spectral accelerations lower than $11 m/s^2$.

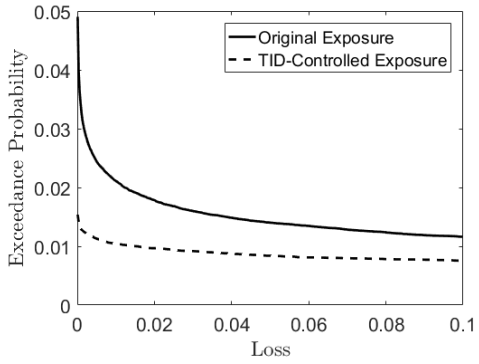

Figure 9. Exceedance probability losses

Figure 9 shows the exceedance probabilities of total losses L for the exposure with the original structures (solid line) and the exposure with the TID-controlled Duffing systems (dashed line). Exceedance probabilities of total losses are consistently lower for the exposure with the TID-controlled Duffing systems.

5. CONCLUSIONS

The goal of this paper was to study the earthquake performance of vibration-controlled systems, in the form of tuned-inerter dampers (TID) in a catastrophe-modelling framework. This framework is used in the insurance industry to evaluate the seismic risk of a group of assets in terms of financial losses. Simplified models for all the main parts of this framework were constructed in order to estimate the risk. Thus, the seismic-hazard part was composed of seismic events characterized by the moment magnitude and epicentral distance, for which local seismic intensities were calculated at every site in the exposure, using a simple ground-motion prediction equation. The exposure part was represented by structures distributed spatially using a uniform distribution. Two types of structures were considered in the form of linear and Duffing SDOF systems. The Duffing SDOF systems were tested with and without TID contribution. The vulnerability part consisted of vulnerability curves, assumed to be identical with fragility curves calculated empirically with the ground-motion records in the NGA-West dataset, for a given maximum absolute displacement threshold. Finally, the seismic risk for the systems with the two types of exposure, i.e. with and without TID-controlled Duffing systems, was evaluated and compared accordingly. Overall, TID-controlled exposure seems to perform better for the entire portfolio of assets, but it may underperform at specific locations in the exposure. Further, more concrete studies are necessary to produce conclusive results regarding the efficiency of such vibration-control systems for seismic risk reduction.

6. ACKNOWLEDGMENTS

The work reported in this paper has been partly supported by the Marie Skłodowska-Curie Actions of the European Union's Horizon 2020 Program under the grant agreement 704679 - PARTNER. This support is gratefully acknowledged.

7. REFERENCES

Abrahamson NA and Silva WJ (1997). "Empirical response spectral attenuation relations for shallow crustal earthquake". *Seismological Research Letters* 68.1, pp. 94–127.

AIR Worldwide, Catastrophe risk engineering solutions, *https://www.air-worldwide.com/Publications/Brochures/documents/AIR-Catastrophe-Risk-Engineering-Solutions/*, last accessed on 26/01/2017.

Giaralis A, Taflanidis A (2017). Optimal tuned mass-damper-inerter (TMDI) designed for seismically excited MDOF structures with model uncertainties based on reliability criteria; *Struct Control Health Monit*. DOI: 10.1002/stc.2082.

Gonzalez-Buelga A, Lazar IF, Jiang ZJ, Neild SA, Inman DJ (2017). Assessing the effect of nonlinearities on the performance of a tuned inerter damper, *Struct Control Health Monit,* vol. 24(3), pp. 1879.

Goda K (2015). "Seismic Risk Management of Insurance Portfolio Using Catastrophe Bonds". *Computer-Aided Civil and Infrastructure Engineering* 30.7, pp. 570–582.

Grossi P and Kunreuther H (2006). Catastrophe modeling: a new approach to managing risk. Ed. by C. C. Patel. Huebner International Series on Risk, Insurance, and Economic Security. New York: Springer.

Lazar IF, Neild SA, Wagg DJ (2014). Using an inerter-based device for structural vibration suppression. *Earthquake Engineering and Structural Dynamics*, **43**(8): 1129-1147.

Lazar IF, Neild SA, Wagg DJ (2016). Vibration suppression of cables using tuned inerter dampers; *Engineering Structures*. Vol **122**: 62-71.

Marian L, Giaralis A (2014). Optimal design of a novel tuned mass-damper–inerter (TMDI) passive vibration control configuration for stochastically support-excited structural systems. *Probabilistic Engineering Mechanics*. Vol **38**: 156 -164.

Poliquin B and Lalonde D (2012). Role of Catastrophe Risk Modelling in Insurance-Linked Securities. Ed. by M. Lane. Alternative (Re)insurance Strategies: 2nd Edition. Ireland: Risk Books.

Smith M.C. (2002). Synthesis of mechanical networks the inerter. *IEEE Transactions on Automatic Control*. Vol **47**: 1648-1662.

Vamvatsikos D and Cornell A (2002). "Incremental dynamic analysis," *Earthquake Engineering and Struct. Dyn.*, vol. 31, pp. 491–514.